Received March 6, 2020, accepted March 18, 2020, date of publication March 23, 2020, date of current version April 7, 2020.

Digital Object Identifier 10.1109/ACCESS.2020.2982697

Target Localization Based on Intermodulation Feedback for Multisine Wireless Power Transmission Using a Time-Modulated Array

YU-QIAN YANG[1,2], **HAO WANG**[1], (Member, IEEE), **HAO ZHANG**[2,3], (Student Member, IEEE), **SHI-FEI TAO**[1], AND **YONG-XIN GUO**[2,4], (Fellow, IEEE)

[1]Department of Communication Engineering, Nanjing University of Science and Technology, Nanjing 210094, China
[2]Department of Electrical and Computer Engineering, National University of Singapore, Singapore 117576
[3]School of Microelectronics, Northwestern Polytechnical University, Xi'an 710072, China
[4]Center for Advanced Microelectronic Devices, National University of Singapore Suzhou Research Institute, Suzhou 215123, China

Corresponding author: Hao Wang (haowang@mail.njust.edu.cn)

This work was supported in part by the National University of Singapore TAP under Grant TAP2002019-04-03, in part by the National Natural Science Foundation of China under Grant 61701240, and in part by the Advanced Research Funds under Grant 61402091603.

ABSTRACT To achieve accurate power feeding to a terminal (e.g. rectenna) in the far-field wireless power transmission (WPT), a new method is proposed to locate the terminal so that the base station can adaptively adjust its beam steering and transmitting power to satisfy the high-efficiency power conversion conditions of the rectifier. In this work, the generated intermodulation (IM) signal at rectenna under multisine incidence is employed to establish the feedback link with the base station. A linear time-modulated array (TMA) is exploited to generate two-tone multisine wave by the optimized modulation sequence thanks to its multi-beam radiation behavior at the base station side. In the terminal end, the IM signal is spontaneously produced due to the nonlinearity of power rectifying under two-tone incidence and employed as the feedback. To highly isolate the two tones and IM signal, a dual linear polarized (DLP) antenna is designed to ensure a compact system design for both sides. By this way, the feedback IM signal carrying the terminal's direction and distance information is sensed by orthogonally polarized antenna pairs. Then the direction of terminal is obtained by the proposed high-accuracy direction of arrival (DoA) estimation method using a multi-baseline TMA, which is realized by a two-stage single-pole-double-throw (SPDT) switching network. Regarding the imperfection of RF switches, a compensation method is proposed. With estimated DoA, the distance between terminal and base station is evaluated based on the received signal strength indicator (RSSI) method. To verify the feedback mechanism, a prototype is fabricated and tested.

INDEX TERMS Time-modulated array (TMA), intermodulation (IM) feedback, directional wireless power transmission.

I. INTRODUCTION

With the development of the fifth-generation (5G) communication technology and the internet of things (IoTs), the number of wireless terminals will predictably grow explosively [1], [2]. Compared with the battery powered solution, the wireless power transmission (WPT) offers a low-cost and flexible solution, and allows the devices to be recharged without the need to plug them in.

The WPT can be classified into two categories as near-field WPT and far-field WPT according to the distance between transmitters and receivers [3]. For far-field WPT, to compensate the propagation path loss as described in the free space, a high-gain antenna array is usually applied. [4], [5]. As long as the beam is steered accurately to the direction of target, the radio frequency (RF) power transmission can attain a high efficiency in radio wave systems over a long range [6]. In mobile scenarios, the transmitter is desired to acquire the change of terminal position and subsequently steer the beam with appropriate transmitted power. Therefore, both the direction and range estimation are required in the far-field WPT application.

Many researchers have taken a lot of efforts on direction finding of the target terminal. One of the main solutions

The associate editor coordinating the review of this manuscript and approving it for publication was Giorgio Montisci.

is to exploit the retrodirectivity technique to automatically track the target by introducing the retrodirective circuit in the receiving (RX) chain. In [7], the authors designed a 2-D retrodirective array using a dipole antenna for indoor WPT. And the retrodirective array for the long-distance case such as the microwave energy harvesting was also employed for tracking purpose [8], [9]. However, this kind of solution suffers from the complex hardware realization. The other kind of method based on channel state information (CSI) learning was discussed from the perspective of communication technology [10]–[12], in which the idea of simultaneous wireless information and power transmission (SWIPT) was proposed. Such a system offers the potential to realize end-to-end communication in complex electromagnetic scenarios, while suffers from the complex waveform design and additional energy division. And the feedback signal training for obtaining the CSI model takes a nonnegligible period of time, which is adverse for a real-time system [13].

By borrowing the idea of harmonic radar detection, the method of direction alignment between TX and RX antennas based on feedback harmonic signals was employed [14]–[18]. Due to the nonlinearity of the rectifier in WPT terminal, multiple harmonic signals could be generated and exploited. For a system operating at f_0, the 3^{rd}-order harmonic $3f_0$ was employed to execute the direction and polarization alignment [14]. And in [16], the 2^{nd}-order harmonic $2f_0$ was utilized to execute the direction of arrival (DoA) estimation. Obviously, a dual-band antenna element or additional element operating at the specific harmonic frequency is required in these cases, which goes against the compact design requirement. In addition, to demodulate the high-order feedback harmonic, a local oscillator at $2f_0$ *or* $3f_0$ needs to be implemented. Fortunately, the corresponding method using in-band feedback signal was employed under two-tone waveform excitation in [17]. The 3^{rd}-order intermodulation (IM) signal operating at $\left(2f_2 - f_1\right)$ or $\left(2f_1 - f_2\right)$ is generated when excited by two-tone waveform f_1, f_2 thanks to the rectifier's nonlinearity. Compared with above out-of-band harmonics, the IM signal experiences a lower path loss and thus additional TX/RX elements are saved. By this way, the transmission range between RF power station and terminal devices is extended.

In this paper, we propose an RF power transmission system with target localization capability based on the IM feedback. In the RF power base station side, the two-tone multisine waveform is employed and generated by using a time-modulated array (TMA). The TMA was introduced as a promising TX beamformer in WPT applications thanks to its sideband radiation (SBR) behavior [18]–[20]. By adding a group of high-speed RF switches in the antenna channel, with modulation frequency f_p, the array is enabled to radiate multiple beams operating at fundamental f_0 and sideband harmonics $f_0 + qf_p$, $q = \pm 1, \pm 2, \ldots$. Thus, the TMA as a multi-frequency multi-beam transmitter is suitable for generating spatial multisine wave signal [21], [22], in which only one signal generator is required. In this work, the positive and negative 1^{st}-order sideband beams ($q = \pm 1$) are exploited to simultaneously feed the target to be charged, while the fundamental and other useless SBRs are suppressed by optimizing the modulation sequence. Once excited by two tones, the IM signal is generated due to nonlinearity of diodes in the rectifier. Thus, the simultaneous wireless charging and feedback generation is achieved without additional power consumption. To further isolate the two-tone wave and feedback IM signal, a dual linearly polarized (DLP) antenna element is employed for downlink (from RF power base station to terminal) and uplink (from terminal to RF power base station) transmission. The two-step observation of terminal's location is proposed. Firstly, the high-accuracy DoA estimation is realized by using alternative short- and long- baseline RX TMA. Under complementary sequence, the terminal's direction is obtained by power ratio of fundamental and SBR of IM signal [23]–[25]. Secondly, the distance estimation is evaluated by the received signal strength indication (RSSI) method. By comparative measurement with the close-in reference point, the target distance can be obtained. With the accurate localization of the terminal, the RF power base station can subsequently adjust the beam steering and transmitted power to feed the desired terminal.

The rest of this paper is organized as follows. In Section II, the overview of the system is illustrated and described. The operating principle is presented in detail in Section III, including mathematical formulas and simulated results. In Section IV, the fabrication and measured results are displayed. Finally, the conclusion and discussion are drawn in Section V.

II. SYSTEM OVERVIEW

To highly isolate the incident two tones and feedbacked IM, dual-polarized (Horizontally Polarized (HP) and Vertically Polarized (VP)) antenna pairs (i.e., HP: TX_1 and RX_1, VP: TX_2 and RX_2) can be employed, which ensures a compact structure by sharing the same antenna aperture for dual polarizations as illustrated by Fig. 1. The proposed system is configured by an RF power base station with TMA and a terminal with rectifier. Both polarization ports of a DLP antenna at the terminal side are connected to the input and isolation ports of a hybrid coupler in the rectifying circuit respectively. At the base station side, the same antenna element is arranged as an array using time modulation architecture in both the TX and RX chains under real-time controlling by a chip of Field Programmable Gate Array (FPGA) board.

In the downlink transmission from the RF power base station to the terminal rectenna, the two-tone wave (f_1, f_2) is of interest and transmitted by the HP antenna pairs. By exploiting the SBRs of TMA, the two-tone wave is produced in an easy and low-cost way. The desired beams are directed into the broadside direction while the higher-order SBRs and sidelobe radiation are suppressed by optimizing the switch-on and duration of each element. The terminal located in the radiation zone of TX array is excited. Due to the property of the hybrid coupler, it is capable of distributing

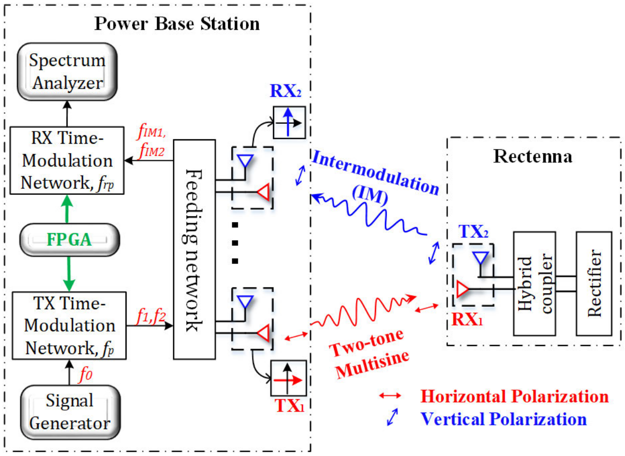

FIGURE 1. Block diagram of the proposed dual-polarized WPT system with simultaneous wireless charging and feedback transmission.

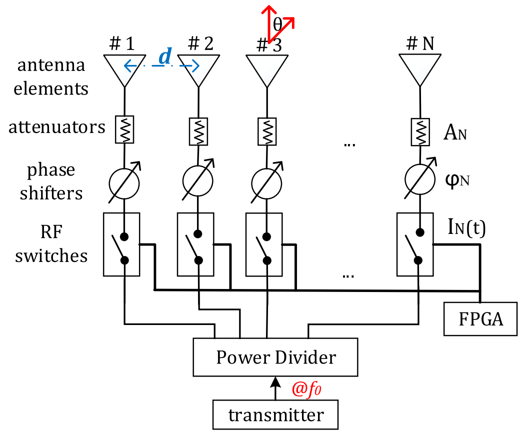

FIGURE 2. Schematic of the N-element linear traditional TMA with one SPST switch in element channel.

two-tone incidences evenly for successive balanced mixing, and simultaneously coupling 3rd-order IM generations $f_{IM1} = (2f_1 - f_2), f_{IM2} = (2f_2 - f_1)$ as feedback signal in two isolated ports. Consequently, the generated IM signal is radiated and sensed by the VP element pairs in the uplink channel. At base station side, the IM signal is mainly observed instead. The reradiated IM signal is received and modulated by a two-stage switching network composed of only two chips of single-pole-double-throw (SPDT) switches. At the same time, the received strength of IM signal is measured to obtain the distance between base station and terminal. Thus, the accurate power beaming can be synthesized at TX side.

III. OPERATING PRINCIPLE

In this section, the operating principle of such a feedback-based transmission system in far-field scenario is explained in detail. Firstly, the operating principle of the TX TMA is given, the generation and optimization processing of the two-tone waveform is illustrated. Then the generation of IM feedback signal is briefly provided as in our previous work [17]. At last, the target localization method based on TMA is discussed. The simulated results are revealed as well to verify the proposed method.

A. BASIS OF THE TMA

The TMA can be classified as one kind of unconventional phased array by adding a group of RF modulators in antenna channels. Traditionally, the modulator is chosen as the RF switch [26]–[28], the variable gain attenuator (VGA) [29], [30], or complex modulation circuits to achieve specific function [20], [31]. From the reported researches, the rectangular pulse modulated TMA using RF switches has been adopted a lot in practical applications compared with the others thanks to its simple realization and easy-to-control. Different from the phased array, the antenna excitation is composed of both static and dynamic compositions, in which the dynamic excitation is behaved by the time-modulator

$$F(\theta, t) = e^{j2\pi f_0 t} \sum_{n=1}^{N} A_n I_n(t) e^{j[(n-1)kd\sin\theta + \varphi_n]} \tag{1}$$

where the k is the wave number at the carrier frequency $f_0 = 2.45\ GHz$, d is the spacing between adjacent elements and $A_n e^{j\varphi_n}$ is the static complex excitation. When the frequency of rectangular time sequence is f_p, the dynamic excitation $I_n(t)$ for nth element is represented as

$$I_n(t) = \begin{cases} 1, & t_{on,n} + mT_P \le t < t_{off,n} + mT_P \\ 0, & others \end{cases} \tag{2}$$

where the parameters t_{on} and t_{off} are respectively switch-on and -off instants of such a rectangular pulse with pulse duration $\tau_n = t_{off,n} - t_{on,n}$ of periodic $T_p = 1/f_p$.

From the perspective of signal processing, the periodic signal in time domain leads to the dispersion of the frequency domain. By Fourier Series analysis, the dynamic excitation can be decomposed as

$$I_n(t) = \sum_{q=-\infty}^{+\infty} i_{n,q} e^{j2\pi q f_p t} \tag{3}$$

where

$$i_{n,q} = \begin{cases} \dfrac{\tau_n}{T_p}, & q = 0 \\ \dfrac{\tau_n}{T_p} sinc\left(\pi q f_p \tau_n\right) e^{-j\pi q f_p (2t_{on,n} + \tau_n)}, & q \neq 0 \end{cases}$$

wherein q is the index of harmonic order. Thus, $I_n(t)$ can be decomposed as an accumulation of infinite orders of harmonic $f_0 + qf_q$, with the equivalent complex excitation $i_{n,q}$. From Eq. (3), it can be easily observed that:

(1) Under the periodic rectangular pulse modulation, the simultaneous multiple beams are distributed at carrier frequency and infinite orders of harmonic, which refers to fundamental and sideband radiations;

(2) The fundamental beam is fixed steering into the broadside direction with amplitude tapering by τ_n;

(3) The sideband beams are generated in pairwise, with equal gain and directing to the symmetrical angle about the broadside. And the gain of different sideband beams varies

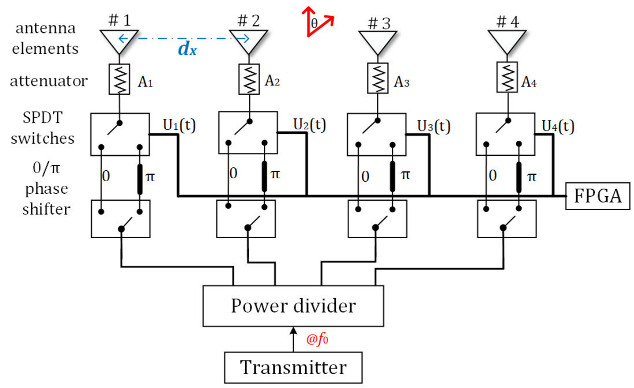

FIGURE 3. Schematic of the 4-element TX array with $0/\pi$ phase modulation using SPDT switches to generate two-tone multisine wave.

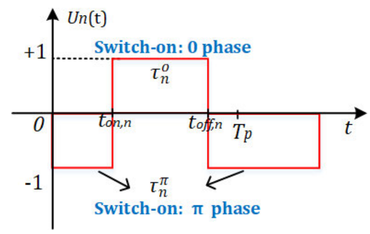

FIGURE 4. Illustration of time sequence achieving $0/\pi$ phase modulation for SPDT switch in nth channel.

with the order q obeying the Sinc function. Both the amplitude and phase can be modulated by τ_n and $t_{on,n}$, by which the amplifier and the phase shifter could be omitted.

As above, the multi-frequency multi-beam radiation performance of TMA is interpreted in detail.

B. GENERATION OF TWO-TONE WAVE USING A TMA

By taking advantage of multi-beam feature of TMA, the two-tone waveform is generated using a TMA with simultaneously two beams pointing to the same direction with equal radiation gain. The 1st-order twin beams as maximum power SBRs are employed as effective radiation beams. To completely counteract the fundamental and even-order SBRs, the $0/\pi$ binary phase modulation technique [26] is used by making the durations of two phase-state equivalent. And the sidelobe radiation is suppressed by optimizing the time sequence.

The schematic of $0/\pi$ modulation architecture is illustrated in Fig. 3 with the time sequence shown in Fig. 4. A four-element linear array by DLP antenna [32] is configured with element adjacent spacing $d_x = \lambda_0/2$, operating at $f_0 = 2.45\ GHz$, $\lambda_0 = c/f_0$. A pair of SPDT switches combined with 0 and π phase delay lines are inserted in element channel. Assume the switch-on instant of 0-phase is $t_{on,n}^o$, the switch-on instant of π-phase is $t_{on,n}^\pi = t_{off,n}^o = t_{on,n}^o + \tau_n^o$ without the switch-off state of switches. To eliminate the fundamental and even-order SBR, the pulse duration of 0- and π-phase is required to be equal, i.e. $\tau_n^o = \tau_n^\pi = \tau_n = T_p/2$. The time sequence under this modulation is modified as

$$U_n(t) = \begin{cases} 1, & t_{on,n}^o + mT_P \le t < t_{on,n}^o + T_P/2 + mT_P \\ -1, & others \end{cases} \tag{4}$$

The excited q th sideband component $a_{n,q}$ after Fourier Series expansion is calculated as Eq. (5). And the array factor in time domain can be represented as Eq. (6) considering the static amplitude excitation. Based on this, the beam direction is regulated by proper $t_{on,n}^o$ and the radiating sidelobe controlled by static amplitude A_n of each element. There the swarm intelligence optimization algorithm Artificial Bee Colony (ABC) algorithm is applied to find the optimal modulating sequence. To suppress the odd-order sideband level (SBL) and the sidelobe level (SLL) of employed sideband beams as much as possible, the objective function $ObjFun$ is formulated including the beam steering accuracy $\alpha\left(t_{on}^o, A\right) = \theta_{t_{on}^o,A} - \theta_o$, the SLL constraint $\beta\left(t_{on}^o, A\right) = SLL_{t_{on}^o,A} - SLL_{des}$, and the beam width limitation $\delta\left(t_{on}^o, A\right) = BW_{t_{on}^o,A} - BW_{des}$ for exploitable beams. And the SBL constraint for higher-order SBRs is $\gamma\left(t_{on}^o, A\right) = SBL_{t_{on}^o,A} - SBL_{des}$. Considering the power decay as the increasement of harmonic order, only the constraints of 3rd- to 5th-order SBLs are considered into the $ObjFun$. Wherein $w_1 \sim w_4$ is the weighting coefficients of each term according to the system requirements, H represents the Heaviside function, and the parameters with subscripted des are desired values. In this case, $SLL_{des} = SBL_{des} = -15\ dB, \theta_o = 0°, BW_{des} = 30°$.

$$a_{n,q}(t_{on}^o) = \begin{cases} 0, & q = 0 \\ \frac{1}{2} sinc\left(\frac{\pi q}{2}\right) e^{-j\pi q f_p \left(2t_{on,n}^o + \frac{T_p}{2}\right)} - \frac{1}{2} sinc\left(\frac{\pi q}{2}\right) e^{-j\pi q f_p \left(2t_{on,n}^o + \frac{3T_p}{2}\right)}, & \\ q = 2K+1, K \in \mathbb{Z} \quad and\ K \neq 0 & \end{cases} \tag{5}$$

$$F'(\theta, t) = e^{j2\pi f_0 t} \sum_{n=1}^{N} A_n \sum_{q=-\infty}^{+\infty} a_{n,q} e^{jk(n-1)d_x sin\theta}, \quad q = 2K+1, K \in \mathbb{Z} \tag{6}$$

$$\begin{aligned} Obj\ Fun\left(t_{on}^o, A\right) = & \sum_{q=-1,+1} [w_1 \frac{\left|\alpha\left(t_{on}^o, A\right)\right|^2}{\left|\theta_{o,q}\right|^2} H\left(\left|\alpha\left(t_{on}^o, A\right)\right|\right) \\ & + w_2 \frac{\left|\beta\left(t_{on}^o, A\right)\right|^2}{\left|SLL_{des,q}\right|^2} H\left(\left|\beta\left(t_{on}^o, A\right)\right|\right) \\ & + w_3 \frac{\left|\delta\left(t_{on}^o, A\right)\right|^2}{\left|BW_{des,q}\right|^2} H\left(\left|\delta\left(t_{on}^o, A\right)\right|\right)] \\ & + w_4 \sum_{q=\pm 3,\pm 5} \frac{\left|\gamma\left(t_{on}^o, A\right)\right|^2}{\left|SBL_{des,q}\right|^2} H\left(\left|\gamma\left(t_{on}^o, A\right)\right|\right) \end{aligned} \tag{7}$$

With the modulation frequency set as $f_p = 300\ kHz$, the two-tone wave is radiated by the 1st-order harmonic $q = -1 : f_1 = f_0 - f_p = 2449.7\ MHz$ and $q = +1 : f_2 = f_0 + f_p = 2450.3 MHz$. By optimizing modulation

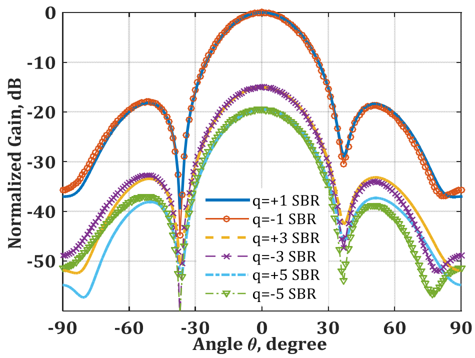

FIGURE 5. Simulated beampatterns of first 5 order sidebands after optimization, with the even-order SBRs eliminated.

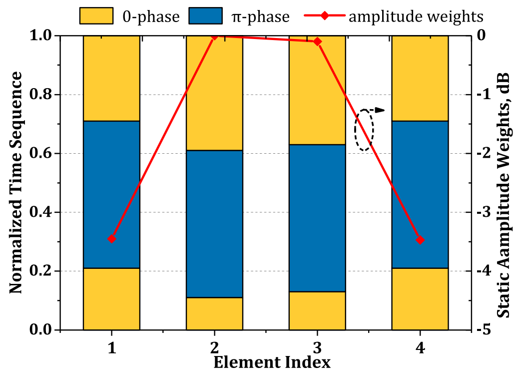

FIGURE 6. Optimized time sequence and static amplitude excitation to generate two-tone waveform.

sequence and amplitude weightings in Fig. 6, the array radiation patterns of 1^{st} $\sim 5^{th}$ SBR are shown in Fig. 5, in which the desired twin-beam of 1^{st}-order show a good consistency. And the SBLs of high orders are also suppressed below -15.34 dB. The experimental verification will be provided in the next section.

C. GENERATION OF INTERMODULATION FEEDBACK

The alignment between the base station and the terminal has been achieved based on harmonics generated from the nonlinearity of the rectifier [14]–[17]. In this proposed system, the 3^{rd}-order harmonics IM operating at $f_{IM1} = (2f_1 - f_2)$ and $f_{IM2} = (2f_2 - f_1)$ are assigned as feedback signal thanks to the lower free space path loss (FSPL) compared with 2^{nd}-order harmonic feedback in [16].

With the optimization process in Section III-B, the two-tone wave (f_1, f_2) is transmitted by HP antennas in the downlink (i.e., TX_1 and RX_1). At the terminal side, the two-tone signal is received by RX_1 and distributed by a hybrid coupler for the successive balanced mixing from two identical diodes D_1 and D_2. According to the nonlinearity of diodes, the IM components (f_{IM1}, f_{IM2}) are generated as incidences at P_2 and P_3, by which two $\lambda_0/4$ shorted stubs at center frequency f_0 can be lumped followed to reject the 2^{nd}-order harmonics at $2f_1$, $2f_2$. Since the frequency offsets between the f_{IM1}, f_{IM2} and f_0 are small, the hybrid coupler is capable of coupling and delivering totally the in-band intermodulation to its isolation

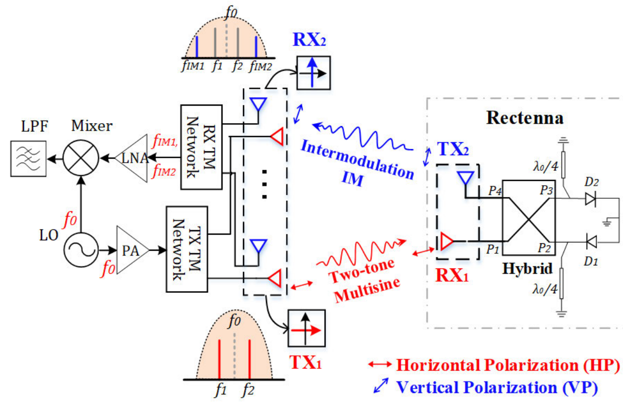

FIGURE 7. Generation of the intermodulation (IM) signal under the two-tone excitation based on a hybrid coupler, in which the two-tone incidence and IM are isolated and sensed by orthogonal antenna pairs.

port P_4 for feedback establishment between the VP antenna pairs (i.e., TX_2 and RX_2).

D. HIGH-ACCURACY DOA ESTIMATION

For the long-distance WPT, the power beaming technology with accurate beam steering is important, which is critical for the transmission efficiency and relating to the compatibility with other systems. The produced IM signal is employed as a feedback signal carrying the terminal's location information, and radiated back to the power base station through VP transmission link. Because the IM signal is separated from the transmitted two tones in both frequency and polarization domain, the captured IM signal at the base station is the most suitable for reading the terminal location information.

In this system, the accuracy-enhanced DoA estimation is obtained by alternative short and long baselines inspired by the Interferometer Direction Finding [25] and following the previous work in [33]. The basis of TMA-based DoA estimation is amplitude-comparison method based on simultaneous sum (Σ) and difference (Δ) beampatterns generated at fundamental and 1st-order sideband beam under a complementary modulating sequence [23], [24].

For a low-cost hardware realization, a SPDT-based two-stage switching network is proposed in our work as shown in Fig. 8. As illustrated in Fig. 8, the 3^{rd} element is utilized for directly power strength measurement of IM feedback. In addition, the elements indexed by #1/#2/#4 are employed to cooperate as multi-baseline interferometer. The long baseline estimation gives a high-accuracy result but with ambiguity, while the short baseline result is low-accuracy with no ambiguity in wide angle range. By combining the results, the accurate results with no ambiguity can be obtained. Meanwhile, the imperfection of preceding stage switch (marked as S1) will lead to the unbalance of input ports of backward stage switch (marked as S2) of the cascaded network in such system and in [25]. This will obviously result in the estimation error and need to be compensated.

The switching network is operating in two states. In **State 1**, the switch S2 is turned into RF1 port, the switch

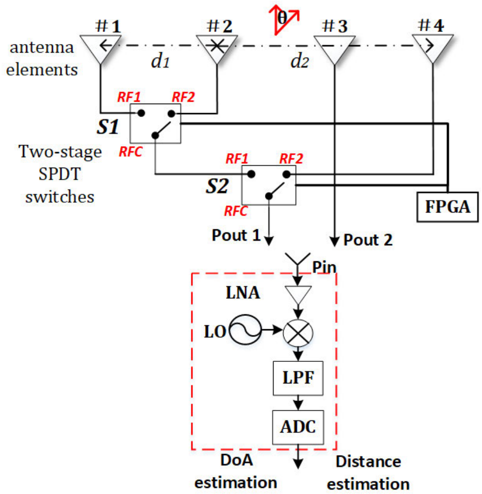

FIGURE 8. Schematic of the 4-element linear TMA with two-stage switching network for target location estimation.

S1 is periodically switched by frequency $f_{rp} = 2\,MHz$, so that the short baseline estimation is achieved by elements #1 and #2 spaced by $d_1 = d_x$ as a rough DoA estimation with no ambiguity. The output marked as P_{out1} after modulation is

$$P_{out1}(t) = s^{IM}(t)\begin{cases}\alpha_s^2 e^{j2\beta_s}, & \{\textbf{State1} \mid \textbf{S1}\ turns\ to\ RF1\}\\ \alpha_s^2 e^{j2\beta_s} e^{jkd_1 sin\theta}, & \{\textbf{State1} \mid \textbf{S1}\ turns\ to\ RF2\}\end{cases} \tag{8}$$

wherein the insertion loss and phase of chosen switch is α_s and β_s respectively, the feedback IM signal is $s^{IM}(t)$. By Fourier Series Decomposition, the normalized fundamental and 1st-order sideband component of IM signal are formulated as

$$\begin{cases} a_{0s}^{IM} = \frac{1}{2}\alpha_s^2 e^{j2\beta_s}\left(1 + e^{jkd_1 sin\theta}\right) \\ a_{1s}^{IM} = -\frac{j}{\pi}\alpha_s^2 e^{j2\beta_s}\left(1 - e^{jkd_1 sin\theta}\right)\end{cases} \tag{9}$$

By measuring the power of received a_{1s}^{IM}, a_{0s}^{IM}, the incident angle under short baseline can be calculated as

$$\tilde{\theta}_s = \arcsin\left(\frac{2}{kd_1} arctan \frac{\pi a_{1s}^{IM}}{2a_{0s}^{IM}}\right) \tag{10}$$

From the Eq. (10), the switch imperfection factor can be cancelled out due to the consistency between two input channels. Since two intermodulation products f_{IM1}, f_{IM2} are with same power levels, only the lower-frequency part is given. The estimated result is offered in Fig. 10 taking the practical radiation performance of the ideal dipole antenna into consideration. The intermediate frequency (IF) is set as 25 MHz, the sampling frequency 200 MHz, and the signal-to-noise ratio (SNR) 30 dB. There is no ambiguity problem in the whole observation span. The error of estimation result is still large, which can be referred to the zoomed figures.

In **State 2**, the improved accuracy estimation is carried out based on long baseline $(d_1 + d_2, d_2 = 2d_x)$ measurement

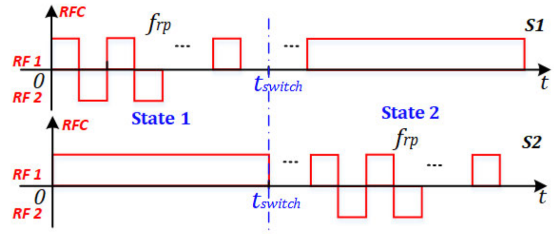

FIGURE 9. Time sequence of the two-stage cascaded switches in Fig. 8 to cooperate as a multi-baseline DoA estimator.

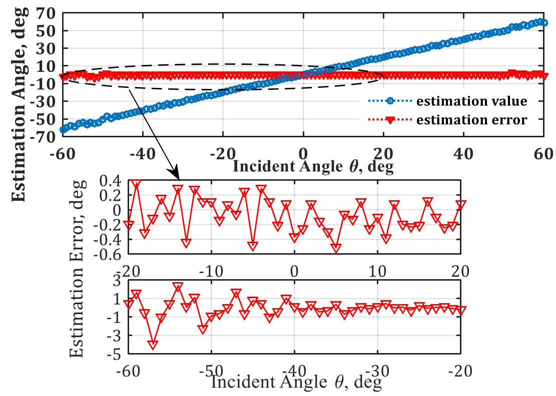

FIGURE 10. The estimated results under short baseline (d_1) estimation, with corresponding zoom in main beam and marginal zones.

using #1 and #4 antennas. The switch S1 is switched into RF1 port, the long baseline estimation is conducted by periodically switching S2 under frequency f_{rp}. The output is then expressed as

$$P'_{out1}(t) = s^{IM}(t)\begin{cases}\alpha_s^2 e^{j2\beta_s}, & \{\textbf{State2} \mid \textbf{S2}\ turns\ to\ RF1\}\\ \alpha_s e^{j\beta_s} e^{jk(d_1+d_2) sin\theta}, & \{\textbf{State2} \mid \textbf{S2}\ turns\ to\ RF2\}\end{cases} \tag{11}$$

The corresponding components should be modified as

$$\begin{cases} a_{0l}^{IM} = \frac{1}{2}\left(\alpha_s e^{j\beta} + e^{jk}(d_1 + d_2) sin\theta\right) \\ a_{1l}^{IM} = \frac{j}{\pi}\left(\alpha_s e^{j\beta} + e^{jk}(d_1 + d_2) sin\theta\right)\end{cases} \tag{12}$$

Under this state, the nonideal characteristics of the switches will affect the estimation result due to the imbalance between the input ports of switch S2. The result with compensation is solved as

$$\tilde{\theta}_l = arcsin\left[\frac{1}{jk(d_1 + d_2)} ln\left(\frac{1+t}{1-t}\right)\alpha_s e^{j\beta_s}\right] + \Phi(m), \tag{13}$$

where $t = \pi a_{1l}^{IM}/j2a_{0l}^{IM}$ is obtained by power measurement at $\boldsymbol{P_{out1}}$ port, $\Phi(m)$ is the ambiguity function with the ambiguity index m determined by $(d_1 + d_2)/(0.5\lambda_0)$, and solved by comparing with short baseline results $\tilde{\theta}_s$.

In this system, the SPDT switch is chosen as ADG918BRM, with the S-parameter $\beta_s = -53°, \alpha_s = 0.708$. Compared with the results under short baseline, it can be observed that the proposed compensation method with

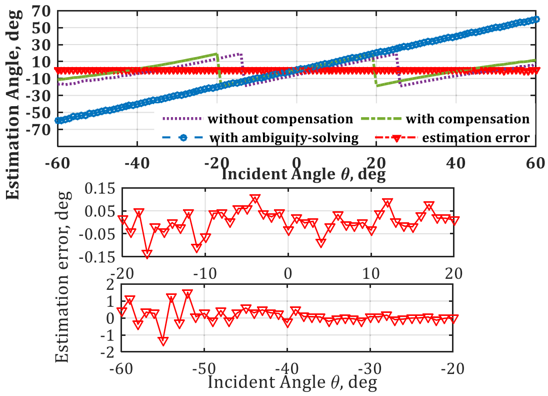

FIGURE 11. The comparative results with/without compensation and ambiguity-solving processing under long baseline ($d_1 + d_2$) estimation.

ambiguity-resolving processing gives a good result in the observation range, as in Fig. 11. And the estimation error in the main beam area of antenna is ideally approaching to zero. This proposed method can be applied in other practical systems with multi-stage switching network.

E. DISTANCE ESTIMATION

With known of direction of the terminal, the distance between the base station and the terminal can be estimated based on the Received Signal Strength Indicator (RSSI) method by measuring the power of f_{IM1} (or f_{IM2}), which is a widely preferred method for its simple hardware realization in distance estimation.

When the TX and RX power are represented by P_t, P_r at the distance R with no obstructions in the line of sight, the received power at terminal side can be formulated by

$$P_r(R,\theta) = \frac{P_t G_t(f_{1,2},\theta)\, G_r(f_{1,2},\theta)\,\lambda^2}{(4\pi)^2 R^2 L_0} \tag{14}$$

wherein G_t is gain of TMA, G_r is gain of rectenna, L_0 represents the loss coefficient of the system in specific scenarios.

In the terminal side, IM signal component is generated as KP_r under the incident power P_r of incident two tones, in which the factor K can be obtained by simulation in ADS software. The IM signal is reradiated back to the base station undergoing additional FSPL, expressed as

$$P_r^{IM}(R,\theta) = \frac{KP_r \cdot G_t(f_{IM},\theta)\, G_r(f_{IM},\theta)\,\lambda_{IM}^2}{(4\pi)^2 R^2 \cdot L_0} \tag{15}$$

Because the difference of antenna gains at IM and two-tone is ignorable (simulated as smaller than 0.03 dB), the relations between received IM power and TX power P_t combining the above equations is

$$P_r^{IM}(R,\theta) = \frac{KP_t G_t^2(f_{IM},\theta)\, G_r^2(f_{IM},\theta)\,{\lambda_{IM}}^4}{(4\pi)^4 R^4 \cdot L_0^2} \tag{16}$$

Thus, the accurate distance R can be calculated with known of transmitted two-tone power P_t, the factor K, and the received power P_r^{IM}. In practice, the comparative measurement is preferred as to counteract the effects of antenna gain

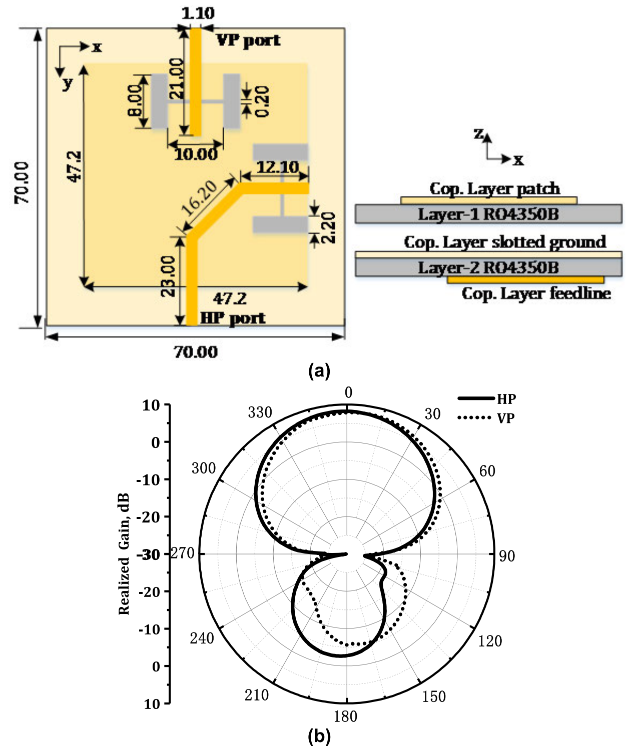

FIGURE 12. (a) Layout (lines dimensions: mm), and (b) radiation pattern of the designed DLP antenna element.

and L_0 by setting a close-in reference point. Take the position of base station TX antenna as the center, select a set of reference points (R_0, θ_k) on the circumference of distance R_0 along incidents θ_k, $k = 1, 2 \ldots K$, and record the received IM power P_{rk}^{IM} at each point under transmitted power P_{t0}. From the Eq. (16), the received power P_r^{IM} is proportional to P_t/R^4, thus, the terminal distance can be obtained by

$$\tilde{R} = \frac{1}{K}\sum\nolimits_k \alpha R_0 \cdot \sqrt[4]{\frac{P_t \cdot P_{rk}^{IM}}{P_{t0} \cdot P_r^{IM}}} \tag{17}$$

with $\alpha = \sqrt{G_t^2\left(f_{IM},\tilde{\theta}\right) G_r^2\left(f_{IM},\tilde{\theta}\right) / G_t^2(f_{IM},\theta_k)\, G_r^2(f_{IM},\theta_k)}$, $\tilde{\theta}$ is the estimated direction in section III-D. By comparing the measured P_r^{IM} with multiple demarcated P_{rk} along incidents θ_k, the distance estimation error can be reduced by averaging.

IV. EXPERIMENTAL VERIFICATION

In order to verify the performance of the proposed method, the experiment is conducted by hardware fabrication. The central frequency is $f_0 = 2.45\ GHz$, TX modulating frequency is $f_p = 300\ kHz$, and RX modulating frequency for DoA estimation is $f_{rp} = 2\ MHz$. The system is divided into four parts including antenna array, TX modulation feeding circuit, RX modulation circuit, and a terminal counterpart. The design and measured results are offered in this section, where the description of terminal is simply given.

A. ANTENNA DESIGN

The DLP antenna element is designed referring to the structure in [32]. The aperture-coupled feeding mechanism is employed in this design for easy fabrication. And for the purpose of array arrangement, the feed ports of two polarized components are designed on the opposite side of radiating patch.

The antenna is composed of two substrate layers with radiating patch and slotted ground separately in each layer. Both the substrates are Rogers RO4350B with thickness 20 mil and $\varepsilon_r = 3.66$. The top layer is the square radiating patch. the ground layer is inserted in the top of the lower substrate with two H-shaped feeding slots, and the feeding lines for two orthogonal polarized electronic fields are placed in the bottom of the lower substrate. The height of air cavity between two substrate layers is 4 mm. The layout of the 4-element linear array is shown in Fig. 13 with the element spacing $d_x = 61.2\ mm$.

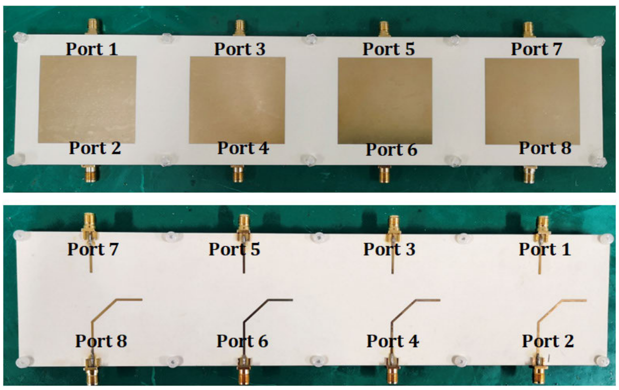

FIGURE 13. Photograph of the 4-element array (top: the top side view, bottom: the bottom view).

The measured reflection and isolation coefficients are displayed in Fig. 14-15, which are generally identical with the simulated results (omitted due to page limit). Fig. 14 shows that the designed array features a good port matching performance with the reflection coefficient below -10 dB over the band of $2.4 - 2.525\ GHz$, which covers the operating frequency band from $f_{\mathrm{IM1}} - f_{rp}(2447.1\ MHz)$ to $f_{\mathrm{IM2}} + f_{rp}(2452.9\ MHz)$. The VP ports numbered as 1,3,5,7 in Fig. 13 are assigned to be RX ports, and the ports isolation influence the accuracy and the sensitivity of the RX channels. In Fig. 15, the measured co-polarized port isolation is over 18 dB, except for the isolation between Port 1 and Port 3 measured as 14.5 dB, which may be caused by the error of fabrication. The cross-polarized port isolation is better than 20 dB, which is beneficial for the isolation between TX and RX channels. From the measurements, the reflection and transmission performance of fabricated array can meet the general requirements, while the slight deterioration will influence the target positioning accuracy to some extent.

B. TX/RX CIRCUIT DESIGN

The fabrication of designed TX and RX modules in Fig.3 and Fig.8 are displayed in Fig. 16. The circuits are fabricated on a 20-mil RO4350B substrate and fixed with an aluminum plate as the supporter to avoid the deformation of

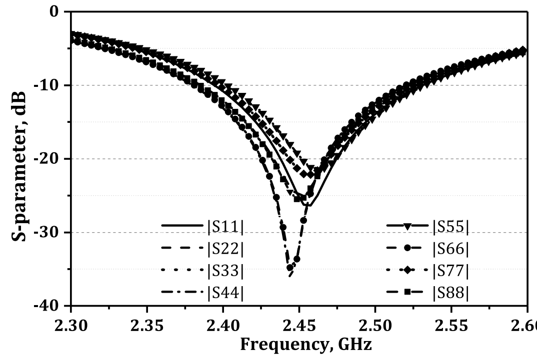

FIGURE 14. The measured reflection coefficients of the fabricated DLP antenna array.

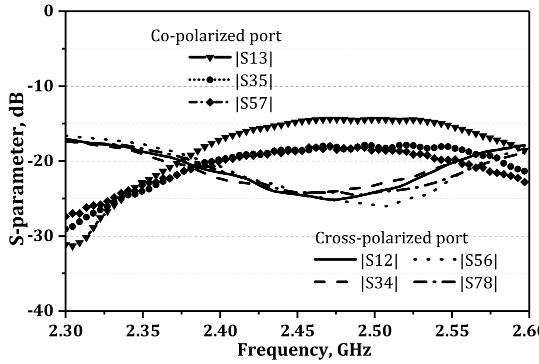

FIGURE 15. The measured transmission coefficients of the fabricated DLP antenna array, including the isolation between co-polarized ports and cross-polarized ports.

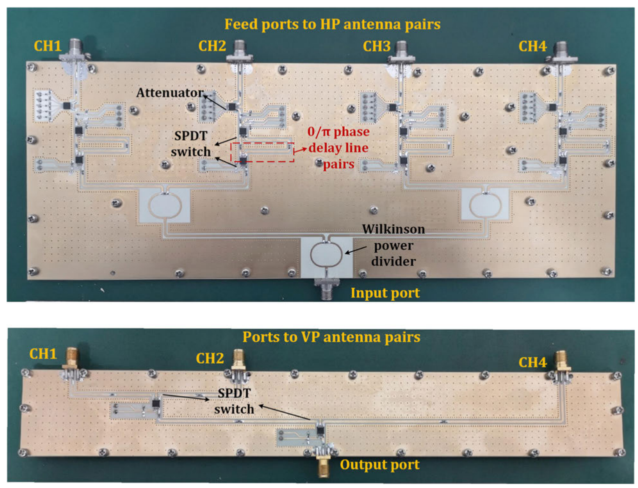

FIGURE 16. Fabrication of the TX (top) and RX (bottom) modulation circuits.

the PCB boards. During the test, the input port of TX power divider is connected to a signal generator Agilent 4432B. The two-stage Wilkinson power divider is for equally power splitting into four element channels. The $0/\pi$ phase delay line pairs are inserted between a couple of SPDT switches ADG918BRM. The attenuator in each channel of TX circuit is HMC306AMS10, which is utilized for amplitude tapering of antenna elements with the attenuation range from $-15.5\ dB$ to $0\ dB$. The feedback signal sensed by VP antenna pairs is received and modulated through the two-stage switching network using two chips of ADG918BRM. And a signal

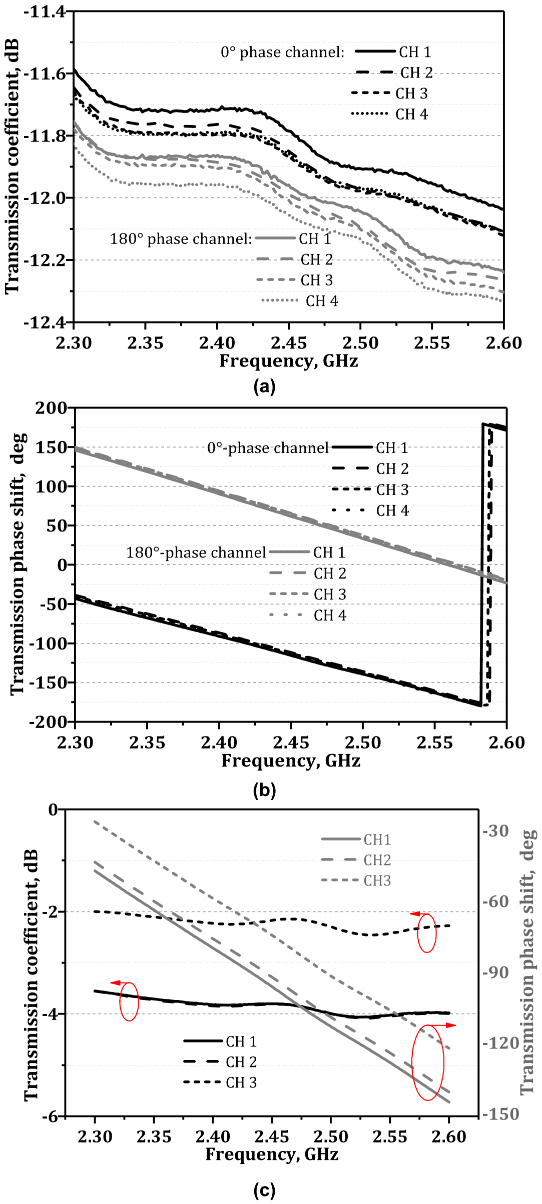

FIGURE 17. The measured: (a) transmission loss and (b) phase shift of TX channels, and (c) transmission loss and phase of RX channels.

analyzer Keysight N9020A MXA is alternatively connected into the combined output port and the port 3 for power measurement. All the control signal and bias of chips are supplied from the XILINX Spartan-6 FPGA.

To acquire the channel transmission performance of realized circuits, the TX board and RX board are tested as a 5-port and 4-port network using Agilent PNA-X Network Analyzer. The measurement of channel insertion loss and phase shift of TX circuit is displayed in Fig. 17 (a)(b), in which the consistency between channels is good. The phase shift under the $0/\pi$ phase modulation of four channels is measured as $[-177.21°, -177.30°, -177.95°, -177.15°]$. And the transmission loss of 180° channel is generally larger than the 0° channel due to additional strip line. The amplitude inconsistency between the channels is considered

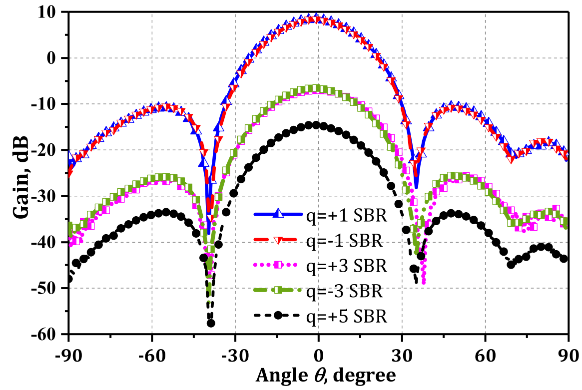

FIGURE 18. The measured sideband radiation (SBR) patterns under optimized sequence and amplitude weighting, with consideration of the measured channel inconsistency in Fig. 17. The SBRs of $q = \pm 1$ with good consistency are exploited to feed the terminal as two tones at $f_1 = f_0 - f_p = 2449.7\ MHz$ and $f_2 = f_0 + f_p = 2450.3\ MHz$.

during re-optimization of TX modulation sequence. The measured transmission parameter of RX channel is displayed in Fig. 17(c). From the results, the realistic insertion loss is corrected as $\beta'_s = -21.87°, \alpha'_s = -1.629\ dB$. And nearly 4° phase difference between channels under **State 1** should be also compensated in DoA estimation.

Finally, the measurement of radiation beampatterns of first-5-sideband under optimized time sequence modulation is conducted with the results shown in Fig. 18, which are in relatively good agreement with simulated results in Fig. 5. And the gain of the array is calibrated using a standard horn antenna. The couple beams of first-order sideband $q = \pm 1$ are simultaneously directing to the broadside direction with the realized gain $G_{q=-1} = 8.39\ dBi$, $G_{q=-1} = 8.44\ dBi$ and $SLL = -19.6\ dB$ under optimized antenna excitation. So that the transmitted sideband signals can be exploited to feed the terminal as two tones (f_1, f_2), at $f_1 = f_0 - f_p = 2449.7\ MHz$ and $f_2 = f_0 + f_p = 2450.3\ MHz$. At the same time, the higher-order SBRs are suppressed to a normalized power of -16.1 dB, which helps to enhance the spectral purity of two-tone signal.

C. RECTIFER DESIGN

To integrate the designed DLP antenna together with two identical rectifiers, the feeding microstrip lines for HP/VP-ports are modified accordingly. Meanwhile, lumped matching solution is introduced in two rectifiers for miniaturized layout, whose detailed structure is shown in Fig. 19(a). Since the input ports of rectifiers are delicately set to 50 Ω (linewidth $w_0 = 1.82\ mm$ on the 32-mil RO4003C) to be integrated with hybrid coupler and feeding microstrip lines as illustrated in Fig. 19(b). And the photograph of fabricated rectenna is shown in Fig. 20. Under incident two-tone signal generated by TMA, the 3rd-order IM will pairwise distributed in $f_{IM1} = 2f_1 - f_2 = 2449.1\ MHz$ and $f_{IM2} = 2f_2 - f_1 = 2450.9\ MHz$.

The rectifier performance is critical for this project. Hence, the power conversion efficiencies (PCEs) and output voltages of a single rectifier are provided in Fig. 21(a). Similarly, only the lower-frequency IM is given in Fig. 21(b) due to the symmetry of two products f_{IM1}, f_{IM2}. As illustrated in Fig. 21,

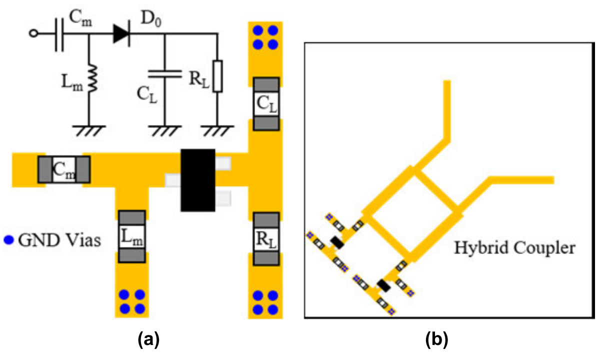

FIGURE 19. (a) Rectifier with lumped matching solution (Insert is the schematic with $C_m = 0.3\ pF$, $L_m = 3\ nH$, $C_L = 22\ uF$, $R_L = 900\ \Omega$, D_0: HSMS286X). (b) Integration of two rectifiers, hybrid coupler and feeding microstrip lines.

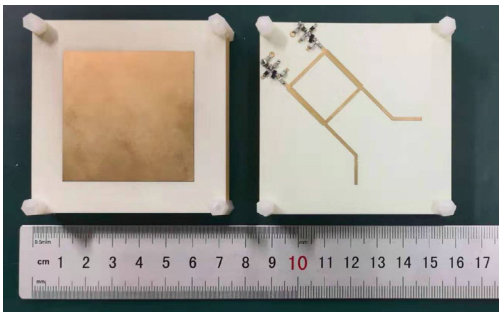

FIGURE 20. Photograph of the designed rectenna (left: the front side, right: the back side).

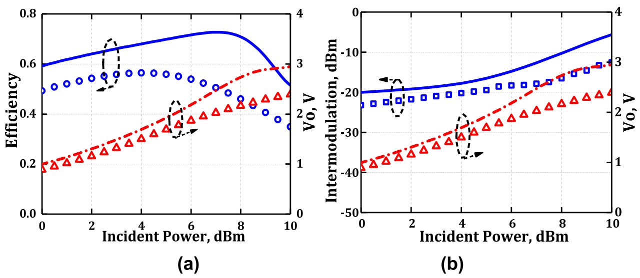

FIGURE 21. The simulated and measured (scattered dots) results of: (a) power conversion efficiencies (PCEs) and output voltages of the single rectifier, (b) lower-frequency intermodulation (IM) of the single rectifier under the two-tone incidence.

the scattered dots represent the measurements, which are generally consistent with simulations. The difference between the measured and simulated results may come from the fabrication variations, cable losses, and an inaccurate diode model in the ADS simulation. Moreover, the intermodulation component is achieved as demonstrated in Fig. 21(b), from which it can be demonstrated that the simultaneous wireless charging and intermodulation generation is realized.

It is noteworthy that the PCEs increase with incident power until the breakdown voltage occurs. And the IM generation is enough for feedback linkbudget establishment without any interference on the single rectifier performance.

D. MEASUREMENT OF DIRECTION AND DISTANCE

To verify the effectiveness of the proposed target localization method based on IM feedback, a proof-of-concept verification experiment is performed using above designed components. The environmental measurement setup is shown in Fig. 22. The RF power station equipped with the DLP antenna array and TX/RX modulation board is fastened on a turntable. A PC with FPGA controller is set to adjust the modulating sequence and amplitude weighting of TX and RX channels. The rectenna as a WPT terminal is placed in the far field zone facing to the antenna array. A CW signal at $f_0 = 2.45\ GHz$ is generated using signal generator Agilent 4432B and fed into input port of TX board. Considering the input power limits of SPDT switches, the feeding power is set as 20 dBm. The two tones (f_1, f_2) at $f_1 = f_0 - f_p = 2449.7\ MHz, f_2 = f_0 + f_p = 2450.3\ MHz$ are generated to feed the rectenna by horizontally polarized TMA under modulation frequency $f_p = 300\ kHz$. At the rectenna side, the vertically polarized IM signal is produced under incident two tones and transmitted back to base station. The feedback IM from rectenna is received by vertically polarized TMA and modulated by frequency $f_{rp} = 2\ MHz$. The output signal after time modulation is fed into an LNA (Mini-Circuits PSA4-5043+) and a signal analyzer Keysight N9020A MXA. With the power measurement of feedback IM a_0^{IM1} and its 1st-order sideband a_1^{IM1}, the terminal's direction is acquired by proposed method in Section III-D. Then the analyzer with LNA is connected into the Port 3 of antenna array to directly measure the reception power strength P_r^{IM1} of signal without time modulation to solve the distance between station and terminal.

Firstly, fixed the distance between power station and terminal (e.g. R= 1.6 m). Change the incident direction from 0°to + 30° by step 5°. The signal power spectrums of incidence from 0°, +15° based on short baseline receiving are plotted in Fig. 23 and the DoA estimation results at instance R= 1.6 m are given in TABLE 1. From the Fig. 23, it can be found that the power of fundamental IM signal decreases as the angle increases, and the variance of sideband power is the opposite. Since the IM products $f_{IM1} = 2f_1 - f_2 = 2449.1\ MHz$ and $f_{IM2} = 2f_2 - f_1 = 2450.9\ MHz$ are with

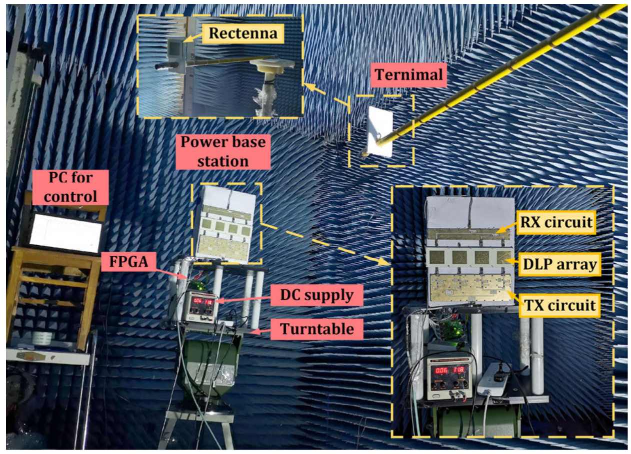

FIGURE 22. The measurement setup of target localization for the far-field WPT system. A TMA with individual TX and RX modulation circuit is equipped for the power base station, and a rectenna is placed as the target terminal.

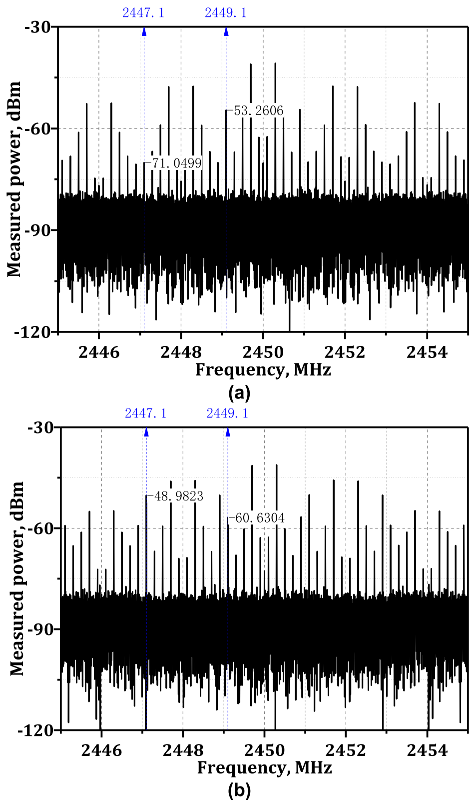

FIGURE 23. The measured spectrums when the feedback incident from: (a) 0°, (b) +15° under the short baseline receiving, with marked IM signal strength a_0^{IM1} at $f_{IM1} = 2449.1$ *MHz* and its 1st-order lower sideband signal a_1^{IM1} at $f_{IM1} - f_{rp} = 2447.1$ *MHz* (the modulation frequency $f_{rp} = 2$ *MHz*).

TABLE 1. DoA estimated results under different incident directions.

Incident angle [deg]	Estimated angle, $\widetilde{\theta}_s$ [deg]	Absolute error [deg]	Estimated angle, $\widetilde{\theta}_l$ [deg]	Absolute error [deg]
0	2.43	2.43	1.22	1.22
5	7.57	2.57	6.12	1.12
10	8.55	1.45	9.64	0.36
15	16.12	1.12	15.76	0.76
20	20.62	0.62	21.18	1.18
25	22.28	2.72	24.13	0.87
30	32.21	2.21	31.93	1.93

same power levels, only the lower-frequency part is marked. By measuring and calculating of the amplitude ratio of fundamental f_{IM1} and its corresponding first sideband component $f_{\mathrm{IM1}} - f_{rp} = 2447.1$ *MHz* (or $f_{\mathrm{IM1}} + f_{rp} = 2445.1$ *MHz*) according to Eq. (10) and Eq. (13), the direction of terminal can be estimated. The switching instant t_{switch} in Fig. 9 is controlled manually in PC to alternatively read the received power under short and long baseline array.

The test is repeated by changing the radial distance R from 1.5 *m* to 2.2 *m*, stepped by 0.1 *m*. And the measurement of reference power indicators P_{rk} at $R_0 = 1.5$ *m* is also conducted for distance estimation. The comparative DoA

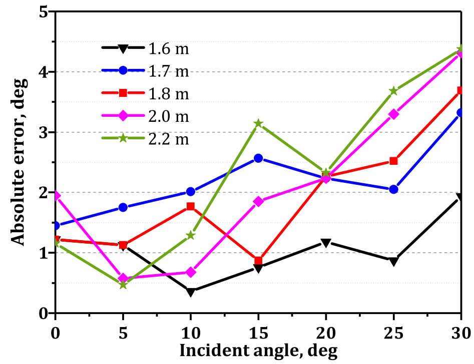

FIGURE 24. The results of high-accuracy DoA estimation based on long baseline receiving when the terminal is located at R= 1.6 *m* to 2.2 *m*.

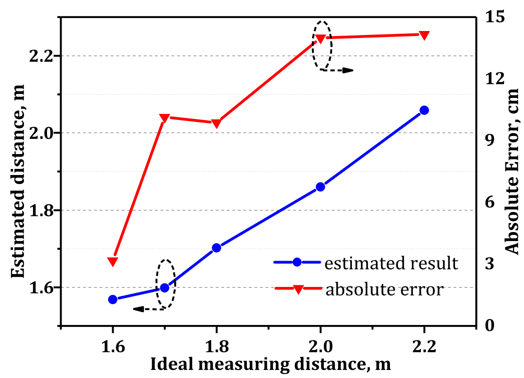

FIGURE 25. The results of target distance estimation.

estimation results are shown in Fig. 24. In general, the measured results deteriorate compared with the simulated results in Fig. 11. This may be caused by the measuring error of spectrum analyzer, especially when the signal power is low. And the unbalance of realized channel will also lead to the degradation, which should be calibrated online. In addition, the local power leakage is a potential influence. And the absolute error tends to be larger as the incident angle and the radial distance increase due to the instability of weak signal.

With direct power measurement of fundamental IM signal P_r^{IM1}, the estimated distance is calculated by Eq. (17), wherein the sampled directions include $\theta_k = [0°, +5°, +10°, +15°, +20°, +25°, +30°]$ under transmitted power $P_{t0} = P_t = 20$ *dBm*. The estimated values are shown in Fig. 25. From the curves, the estimated results are basically in line with the ideal distance in the near range with the accuracy within 15 cm. The absolute error is non-negligible, especially at the distant measuring points due to the weakness of signal power. The deterioration results from the error of DoA estimation as in Fig. 24 and the limitation of RSSI-based distance estimation technique. The measurement accuracy can be improved as long as the reference points are enough.

Generally, the measured results show the capability of proposed method to find the location of the terminal roughly. The accuracy can be enhanced by adding EMC design of RF circuits, the design of high-isolated dual-polarized antenna, utilization of high-accuracy measurement devices, and accurate calculation without approximation. And the real-time localization of terminal can be achieved by corresponding software design embedded in the system. On this basis, the accurate power beaming can be formed by optimal time sequence design of the TX TMA, which can be further discussed in the future work.

V. CONCLUSION AND DISCUSSION

For the far-field WPT, it is important for the base station to accurately track the terminal in real time. Regarding of the movement of terminal, it is important for the base station to adjust the transmitting power to compensate the propagation loss, so that the terminal can operate in a high-efficiency status within the specific range of incident power. In this paper, the idea to locate wireless terminal by spontaneously produced IM under two-tone incidence is proposed for directional WPT application. The TMA is firstly realized as the multisine transmitter thanks to its simultaneous multi-beam characteristic. In fact, it can also be utilized to achieve diverse waveform by specific modulation circuit design.

Under the two-tone incidence, the IM signal is generated and delivered into the isolation port of hybrid coupler in rectifier circuit. The generated IM is employed as feedback and transmitted by orthogonally polarized antenna pairs, by which the isolation between two tones and IM is enhanced. Then the direction and distance estimation based on the feedback signal are achieved by analyzing the received power spectrum using the TMA receiver. Based on this, the optimal power beaming strategy can be adapted with optimal TX time modulation to accurately feed the terminal.

To verify the performance of such a method, a fully functional prototype is designed and fabricated. Both simulation and measurement show that the proposed method is appealing to be applied in far-field directional powering applications once the estimation accuracy is ensured. The improvements to enhance the accuracy may include:

(1) the improvement of port isolation of the DLP antenna array to enhance the isolation between downlink and uplink channels.

(2) the optimization of channel consistency of RF circuits, and the EMC design should be considered to reduce the coupling of unwanted power.

(3) the selection of high-performance RF switches, with high off-isolation, and short rise/fall time, especially for RX modulation network.

(4) the reliable method of channel calibration, which helps to enhance the estimation accuracy a lot.

REFERENCES

[1] Q. Liu, K. S. Yildirim, P. Pawełczak, and M. Warnier, "Safe and secure wireless power transfer networks: Challenges and opportunities in RF-based systems," *IEEE Commun. Mag.*, vol. 54, no. 9, pp. 74–79, Sep. 2016.

[2] A. Costanzo and D. Masotti, "Smart solutions in smart spaces: Getting the most from far-field wireless power transfer," *IEEE Microw. Mag.*, vol. 17, no. 5, pp. 30–45, May 2016.

[3] N. B. Carvalho, "Europe and the future for WPT," *IEEE Microw. Mag.*, vol. 18, no. 4, pp. 56–87, Jun. 2017.

[4] P. S. Yedavalli, T. Riihonen, X. Wang, and J. M. Rabaey, "Far-field RF wireless power transfer with blind adaptive beamforming for Internet of Things devices," *IEEE Access*, vol. 5, pp. 1743–1752, Mar. 2017.

[5] K. W. Choi, P. A. Rosyady, L. Ginting, A. A. Aziz, D. Setiawan, and D. I. Kim, "Theory and experiment for wireless-powered sensor networks: How to keep sensors alive," *IEEE Trans. Wireless Commun.*, vol. 17, no. 1, pp. 430–444, Jan. 2018.

[6] N. Shinohara, "Beam efficiency of wireless power transmission via radio waves from short range to long range," *J. Electromagn. Eng. Sci.*, vol. 10, no. 4, pp. 224–230, Dec. 2010.

[7] Y. Li and V. Jandhyala, "Design of retrodirective antenna arrays for short-range wireless power transmission," *IEEE Trans. Antennas Propag.*, vol. 60, no. 1, pp. 206–211, Jan. 2012.

[8] F. E. Little, S. J. Kokel, C. T. Rodenbeck, K. Chang, G. D. Arndt, and P. H. Ngo, "Development of a retrodirective control transmitter for wireless power transmission," *URSI Radio Sci. Bull.*, no. 311, pp. 38–46, Dec. 2004.

[9] S. Sasaki, K. Tanaka, and K.-I. Maki, "Microwave power transmission technologies for solar power satellites," *Proc. IEEE*, vol. 101, no. 6, pp. 1438–1447, Jun. 2013.

[10] A. Costanzo and D. Masotti, "Energizing 5G: Near- and far-field wireless energy and data trantransfer as an enabling technology for the 5G IoT," *IEEE Microw. Mag.*, vol. 18, no. 3, pp. 125–136, May 2017.

[11] M. Zhang, K. Cumanan, L. Ni, H. Hu, A. G. Burr, and Z. Ding, "Robust beamforming for AN aided MISO SWIPT system with unknown eavesdroppers and non-linear EH model," in *Proc. IEEE Globecom Workshops (GC Wkshps)*, Abu Dahbi, United Arab Emirates, Dec. 2018, pp. 1–7.

[12] J. Xu and R. Zhang, "Energy beamforming with one-bit feedback," *IEEE Trans. Signal Process.*, vol. 62, no. 20, pp. 5370–5381, Oct. 2014.

[13] Y. Zeng and R. Zhang, "Optimized training design for wireless energy transfer," *IEEE Trans. Commun.*, vol. 63, no. 2, pp. 536–550, Feb. 2015.

[14] H. Zhang, Y.-X. Guo, S.-P. Gao, Z. Zhong, and W. Wu, "Exploiting third harmonic of differential charge pump for wireless power transfer antenna alignment," *IEEE Microw. Wireless Compon. Lett.*, vol. 29, no. 1, pp. 71–73, Jan. 2019.

[15] X. Gu, N. N. Srinaga, L. Guo, S. Hemour, and K. Wu, "Diplexer-based fully passive harmonic transponder for Sub-6-GHz 5G-compatible IoT applications," *IEEE Trans. Microw. Theory Techn.*, vol. 67, no. 5, pp. 1675–1687, May 2019.

[16] T. Mitani, S. Kawashima, and N. Shinohara, "Direction-of-arrival estimation by utilizing harmonic reradiation from rectenna," in *Proc. IEEE Wireless Power Transf. Conf. (WPTC)*, Montreal, QC, Canada, Jun. 2018, pp. 1–4.

[17] H. Zhang, S.-P. Gao, T. Ngo, W. Wu, and Y.-X. Guo, "Wireless power transfer antenna alignment using intermodulation for two-tone powered implantable medical devices," *IEEE Trans. Microw. Theory Techn.*, vol. 67, no. 5, pp. 1708–1716, May 2019.

[18] D. Masotti, A. Costanzo, M. Del Prete, and V. Rizzoli, "Time modulation of linear arrays for real-time reconfigurable wireless power transmission," *IEEE Trans. Microw. Theory Techn.*, vol. 64, no. 2, pp. 331–342, Feb. 2016.

[19] D. Masotti and A. Costanzo, "Time-based RF showers for energy-aware power transmission," in *Proc. 11th Eur. Conf. Antennas Propag. (EUCAP)*, Paris, France, Mar. 2017, pp. 783–787.

[20] Y.-Q. Yang, H. Wang, and Y.-X. Guo, "A time-modulated array with digitally preprocessed rectangular pulses for wireless power transmission," *IEEE Trans. Antennas Propag.*, early access, Jul. 26, 2019, doi: 10.1109/TAP.2019.2930135.

[21] F. Mani, D. Masotti, and A. Costanzo, "Exploitation of time modulated arrays for multisine power transmission," in *Proc. IEEE 29th Annu. Int. Symp. Pers., Indoor Mobile Radio Commun. (PIMRC)*, Bologna, Italy, Sep. 2018, pp. 301–305.

[22] F. Mani, D. Masotti, and A. Costanzo, "Nonlinear design of time-modulated array for medium power multisine wireless power transfer," in *Proc. IEEE Topical Conf. Wireless Sensors Sensor Netw. (WiSNet)*, Orlando, FL, USA, Jan. 2019, pp. 1–4.

[23] A. Tennant and B. Chambers, "A two-element time-modulated array with direction-finding properties," *IEEE Antennas Wireless Propag. Lett.*, vol. 6, pp. 64–65, 2007.

[24] C. He, X. Liang, Z. Li, J. Geng, and R. Jin, "Direction finding by time-modulated array with harmonic characteristic analysis," *IEEE Antennas Wireless Propag. Lett.*, vol. 14, pp. 642–645, 2015.

[25] C. He, J. Chen, X. Liang, J. Geng, W. Zhu, and R. Jin, "High-accuracy DOA estimation based on time-modulated array with long and short baselines," *IEEE Antennas Wireless Propag. Lett.*, vol. 17, no. 8, pp. 1391–1395, Aug. 2018.
[26] J. Yang, W. Li, and X. Shi, "Phase modulation technique for four-dimensional arrays," *IEEE Antennas Wireless Propag. Lett.*, vol. 13, pp. 1393–1396, 2014.
[27] L. Poli, P. Rocca, L. Manica, and A. Massa, "Pattern synthesis in time-modulated linear arrays through pulse shifting," *IET Microw., Antennas Propag.*, vol. 4, no. 9, pp. 1157–1164, Sep. 2010.
[28] C. He, X. Liang, B. Zhou, J. Geng, and R. Jin, "Space-division multiple access based on time-modulated array," *IEEE Antennas Wireless Propag. Lett.*, vol. 14, pp. 610–613, 2015.
[29] R. Maneiro-Catoira, J. C. Bregains, J. A. Garcia-Naya, and L. Castedo, "Enhanced time-modulated arrays for harmonic beamforming," *IEEE J. Sel. Topics Signal Process.*, vol. 11, no. 2, pp. 259–270, Mar. 2017.
[30] R. Maneiro-Catoira, J. Bregains, J. A. Garcia-Naya, and L. Castedo, "Analog beamforming using time-modulated arrays with digitally preprocessed rectangular sequences," *IEEE Antennas Wireless Propag. Lett.*, vol. 17, no. 3, pp. 497–500, Mar. 2018.
[31] A.-M. Yao, W. Wu, and D.-G. Fang, "Single-sideband time-modulated phased array," *IEEE Trans. Antennas Propag.*, vol. 63, no. 5, pp. 1957–1968, May 2015.
[32] H. Sun and W. Geyi, "A new rectenna with all-polarization-receiving capability for wireless power transmission," *IEEE Antennas Wireless Propag. Lett.*, vol. 15, pp. 814–817, 2016.
[33] Y.-Q. Yang, H. Wang, H. Zhang, and Y.-X. Guo, "A compensation method for switches imperfection in direction finding system using time-modulated arrays," in *Proc. IEEE Asia–Pacific Microw. Conf. (APMC)*, Singapore, 2019, pp. 1399–1401.

YU-QIAN YANG was born in Taiyuan, China, in 1991. She received the B.S. degree in communication engineering from the Nanjing University of Science and Technology (NUST), Nanjing, China, in 2014. She is currently pursuing the Ph.D. degree in electromagnetic fields and microwave technology with the Department of Communication Engineering.

She was a Visiting Ph.D. Student with the Department of Electrical and Computer Engineering, National University of Singapore (NUS), Singapore, from September 2017 to September 2018. Her research interests include antenna arrays, unconventional phased array design, and intelligent optimization algorithm.

HAO WANG (Member, IEEE) received the B.S. and Ph.D. degrees in electrical engineering from the Nanjing University of Science and Technology, Nanjing, China, in 2002 and 2009, respectively.

He is currently an Associate Professor with the School of Electronic and Optical Engineering, Nanjing University of Science and Technology (NUST). His current research interests include microstrip antennas for wireless communications, terminal antenna subsystem for compass navigation satellite systems, antenna subsystem design, low-temperature co-fired ceramics-based system-on-package technology, and antennas in package. He also serves as a Reviewer for many international journals, such as the IEEE Transactions on Antennas and Propagation and the IEEE Antennas and Wireless Propagation Letters.

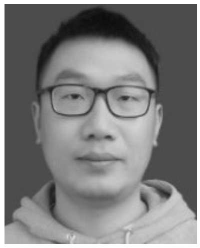

HAO ZHANG (Student Member, IEEE) was born in Xuzhou, China. He received the B.E. and Ph.D. degrees in electronic engineering from the Nanjing University of Science and Technology (NUST), Nanjing, China, in 2014 and 2019, respectively.

From 2015 to 2018, he was a Joint Ph.D. Candidate with the Department of Electrical and Computer Engineering, National University of Singapore. He is currently an Associate Professor with the School of Microelectronics, Northwestern Polytechnical University, Xi'an, China. His current research interests include wireless power transmission and RF energy harvesting, MMIC, flexible microelectronics and sensors for biomedical, and healthcare applications. He was a recipient of the MTT-S Travel Grant Award of Asian Pacific Microwave Conference (APMC), in 2019. He also serves as a Reviewer for many international journals, such as the IEEE Transactions on Microwave Theory and Techniques, the *IEEE Microwave Magazine*, the IEEE Microwave and Wireless Components Letters, and the IEEE Journal of Electromagnetics, RF, and Microwaves in Medicine and Biology.

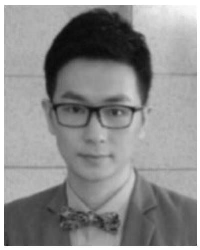

SHI-FEI TAO received the B.Sc. and Ph.D. degrees from the Department of Communication Engineering, Nanjing University of Science and Technology (NUST), Nanjing, China, in 2008 and 2014, respectively.

From 2015 to 2016, he was a Postdoctoral Research Associate in electric and computer engineering with Northeastern University, Boston, MA, USA. Since 2017, he has been with the Nanjing University of Science and Technology, where he was a Lecturer. He is currently an Associate Professor with the Department of Communication Engineering, NUST. His current research interests include computational electromagnetics, antennas, and electromagnetic scattering and radiation.

YONG-XIN GUO (Fellow, IEEE) received the B.Eng. and M. Eng. degrees from the Nanjing University of Science and Technology, Nanjing, China, and the Ph.D. degree from the City University of Hong Kong, all in electronic engineering, in 1992, 1995, and 2001, respectively.

He is currently a Full Professor with the Department of Electrical and Computer Engineering, National University of Singapore (NUS). Concurrently, he is the Director of the Center of Advanced Microelectronic Devices, NUS Suzhou Research Institute. He has authored or coauthored over 460 international journal articles and conference papers and four book chapters. He holds over 30 granted/filed patents in USA, China, and Singapore. His current research interests include antennas, wireless power, RF and millimeter-wave sensing, MMIC modeling and design for wireless communications, the IoTs, and biomedical applications. He has graduated 13 Ph.D. students at NUS.

Dr. Guo was a recipient of the 2020 IEEE Microwave and Wireless Components Letters Tatsuo Itoh Prize of the IEEE Microwave Theory and Techniques Society (MTT-S). He is the Chair of the IEEE AP-S Technical Committee on Antenna Measurement, from 2018 to 2020. He has served as the General Chair/Co-Chair for the IEEE MTT-S IMWS-AMP 2020, APMC 2019, AWPT 2017, ACES-China 2017, the IEEE MTT-S IMWS-AMP 2015, and the IEEE MTT-S IMWS-Bio 2013. He has served as the Technical Program Committee (TPC) Co-Chair for the IEEE MTT-S IMBioC 2020, IMWS-AMP 2017/2019, and RFIT 2009. He has served as the IEEE Fellow Evaluation Committee for the IEEE Engineering in Medicine and Biology Society, from 2019 to 2020. He is serving as an Associate Editor for the IEEE Journal of Electromagnetics, RF and Microwave in Medicine and Biology, and the *IEEE Antennas and Propagation Magazine*.